NACA RM E57D16

NACA

RESEARCH MEMORANDUM

PERFORMANCE COMPARISON AT MACH NUMBERS 1.8 AND 2.0 OF FULL-SCALE AND QUARTER-SCALE TRANSLATING-SPIKE INLETS

By Donald P. Hearth, Bernhard H. Anderson, and Murray Dryer

Lewis Flight Propulsion Laboratory
Cleveland, Ohio

October 21, 1957
Declassified August 9, 1963

NATIONAL ADVISORY COMMITTEE
FOR AERONAUTICS
WASHINGTON

NACA RM E57D16

NATIONAL ADVISORY COMMITTEE FOR AERONAUTICS

RESEARCH MEMORANDUM

PERFORMANCE COMPARISON AT MACH NUMBERS 1.8 AND 2.0 OF FULL-SCALE AND QUARTER-SCALE TRANSLATING-SPIKE INLETS

By Donald P. Hearth, Bernhard H. Anderson
and Murray Dryer

SUMMARY

The performance of a full-scale translating-spike inlet was obtained at Mach numbers of 1.8 and 2.0 and at angles of attack from 0° to 6°. Comparisons were made between the full-scale production inlet configuration and a geometrically similar quarter-scale model.

The inlet pressure-recovery, cowl pressure-distribution, and compressor-face distortion characteristics of the full-scale inlet agreed fairly well with the quarter-scale results. In addition, the results indicated that bleeding around the periphery ahead of the compressor-face station improved pressure recovery and compressor-face distortion, especially at angle of attack.

INTRODUCTION

Full-scale-inlet performance estimates are usually determined from data derived from small-scale tests. To fully evaluate inlet configurations, it is desirable to investigate the full-scale production version at the simulated flight conditions in order to determine any inlet performance differences between the full-scale and quarter-scale versions.

Included herein are the results of an investigation conducted in the 10- by 10-foot supersonic wind tunnel at the NACA Lewis laboratory on a full-scale production nacelle. The axial-symmetric inlet employed a translating spike and a blunt lip. Two versions of the inlet have been studied in quarter scale, and the results are reported in references 1 and 2. This report discusses the inlet performance results and compares them with the results of the geometrically similar quarter-scale model (ref. 2). The inlet stability characteristics of the full-scale and quarter-scale configurations are included in reference 3. Inlet performance and compressor-face distortions for another full-scale configuration are reported in references 4 and 5.

Data were obtained at angles of attack of 0°, 3°, and 6° and at free-stream Mach numbers of 1.8 and 2.0. Testing at free-stream Mach numbers below the facility limit of 2.0 was achieved by the use of compression plates located upstream of the nacelle.

SYMBOLS

The following symbols are used in this report:

A	flow area, sq ft
A_c	capture area, 5.0741 sq ft
C_d	drag coefficient, D/q_0A_c
C_p	pressure coefficient, $\frac{p - p_0}{q_0}$
D	drag, lb
M	Mach number
m	mass flow, slugs/sec
m_1	total inlet mass flow, $m_2 + m_s$, slugs/sec
P	total pressure, lb/sq ft
p	static pressure, lb/sq ft
q	dynamic pressure, $\frac{\gamma}{2} pM^2$, lb/sq ft
R	radius
$\frac{w\sqrt{\theta}}{\delta}$	corrected airflow parameter, lb/sec
w	weight flow, lb/sec
α	angle of attack, deg
γ	ratio of specific heats for air, 1.4
δ	ratio of total pressure to NACA standard sea-level static pressure of 2116 lb/sq ft
θ	ratio of free-stream total temperature to NACA standard sea-level static temperature of 518.7° R

θ_l spike-position parameter (angle between diffuser axis and line joining apex of cone to vertical tangent of cowl lip), deg

Subscripts:

a additive

av average

c cowl pressure

max maximum

min minimum

s subinlet

0 free stream

1 cowl lip station

2 compressor-face station

APPARATUS AND PROCEDURE

The inlet nacelle configuration was installed in the 10- by 10-foot supersonic wind tunnel as shown in figure 1(a). Data were obtained at free-stream Mach numbers of 2.0 and 1.8 and at angles of attack of 0°, 3°, and 6°. Testing the model at Mach numbers below the facility limit of 2.0 was achieved by means of compression plates mounted as shown in figure 1(b). The principle of operation of these compression plates is the same as that discussed in reference 6.

The inlet consisted of a 25° half-angle spike, which could be translated for airflow regulation, and a blunt-lip cowl. Details of the inlet and compressor-face instrumentation are shown in figure 2. The flow-area variation (fig. 3) and the internal geometry of the inlet (with the exception of the subinlets) were the same as those of the quarter-scale-inlet model reported in reference 2. Although the outside contour of the quarter-scale model was not the same as the bottom of the production nacelle, it was identical to the top of the nacelle (fig. 2(a)). The bulge on the bottom of the full-scale nacelle provided space for engine accessories. Static-pressure instrumentation was installed on the spike and cowl lip to provide additive and cowl pressure drag.

The full-scale inlet had three subinlets mounted around the periphery of the main inlet (fig. 4). These inlets provided air for engine

oil coolers and the ejector. For the cold-flow configuration, however, the subinlet airflow was bled out of the base around the exit plug. The subinlet throats were choked at all times, thus simulating the condition with engine operation. Pressure instrumentation was installed in all three subinlets. The pressure measurements indicated that each subinlet handled about 3 percent of the total main-inlet flow.

Airflow was varied with a choked exit plug and was measured by the static-pressure survey at the plug entrance shown in figure 1. A flow coefficient of 0.978 was used.

RESULTS AND DISCUSSION

The performance of the subinlets during critical operation of the main inlet is presented in figure 5. When the spike was retracted at zero angle of attack, the pressure recovery decreased rapidly because of the lower energy air around the main-inlet periphery. As the angle of attack was increased, the bottom subinlet handled extremely low-energy air as anticipated. Most of the data was taken with the subinlets open; however, a spot check was made with the subinlets closed at the downstream end. A comparison of the profiles in figure 6 indicates that the subinlets removed low-energy air around the periphery, thereby improving both distortion and the mean total pressure. At a 6° angle of attack, flow separation from the bottom of the cowl was removed by the bottom subinlet.

Figures 7 and 8 present the inlet performance data for free-stream Mach numbers of 1.8 and 2.0 at angles of attack of 0°, 3°, and 6°. The results are presented in terms of total inlet (engine plus subinlets) mass flow and are compared with the quarter-scale results (ref. 2). If the experimental accuracy and the effect of the subinlets are considered, the agreement is good. The effect of spike extension on peak pressure recovery (equal to the critical value for this inlet configuration) and on critical flow distortion are shown in figure 9. As noted previously, the performance of the full-scale configuration agreed closely with the quarter-scale results. However, the full-scale-inlet pressure recovery did not increase as rapidly with spike extension as did that of the quarter-scale model. The effectiveness of the subinlets in reducing distortion and in increasing pressure recovery, especially at angle of attack, is apparent in figures 7 and 9(a).

The inlet performance data presented in figures 5 to 9 were obtained at a free-stream Reynolds number of 6.8×10^6 (based on cowl-lip diameter). Varying the Reynolds number from 1.7×10^6 to 9.2×10^6 did not affect the inlet performance when the inlet was not pulsing. The effect of Reynolds number on inlet stability is reported in reference 3.

Because of the blunt cowl lip of the inlet, the cowl pressure drag assumes added importance. A comparison of representative cowl pressure distribution on top of the nacelle for the full-scale inlet and the quarter-scale model is given in figure 10. Reasonably good agreement was obtained, and therefore the integrated cowl pressure drags might be expected to agree. However, as shown in figure 11, the pressure drags obtained in this test were lower than those reported in reference 2. This difference is probably due to more accurate fairing of the pressure distribution curves near the stagnation point for the full-scale inlet. Because of differences in the sizes of the two configurations, more instrumentation for the full-scale configuration was installed in this important region. The measured variation of the stagnation point on the full-scale inlet is presented in figure 12.

Additive drag was computed by means of the method outlined in reference 7. Pressures on the spike and cowl were measured and integrated, while pressure recoveries at the lip were assumed. Allowance for the effect of normal- and oblique-shock locations on the assumed pressure recovery was made. In addition, an average flow direction at the cowl was used. The results are presented in figure 13 and are compared with the theoretical normal-shock and oblique-shock values (ref. 7). For a given spike position, the drag increased with spillage at the same rate as the theoretical normal-shock drag. However, for critical operation, the additive drag decreased as the spike was extended to a spike-position parameter of 38.3°, even though the amount of spillage increased. This can be seen qualitatively in figure 14, which shows that, as the spike was extended, the blunt-lip detachment shock moved closer to the cowl lip, thus reducing the amount of normal-shock spillage. The associated normal-shock additive-drag decrease apparently was large enough to more than compensate for the increase in oblique-shock additive drag.

SUMMARY OF RESULTS

The following results were observed in an investigation of a full-scale translating-spike inlet at free-stream Mach numbers of 1.8 and 2.0.

1. Bypassing air from around the periphery ahead of the engine-face station resulted in an increase in inlet pressure recovery and a decrease in distortion, especially at angle of attack.

2. Inlet pressure recovery and compressor-face distortion agreed fairly well between the full-scale production inlet and a geometrically similar quarter-scale model.

3. Although cowl pressure distribution for the quarter-scale and full-scale inlet configurations agreed reasonably well, the integrated

pressure drags were somewhat different. This resulted from more accurate fairing of the pressure distribution curves in the region of the stagnation point for the full-scale configuration.

4. Measured critical additive drag decreased with spike extension even though the total spillage was increased. This effect was due to a decrease in normal-shock spillage around the blunt lip as the spike was extended.

Lewis Flight Propulsion Laboratory
National Advisory Committee for Aeronautics
Cleveland, Ohio, May 20, 1957

REFERENCES

1. Gorton, Gerald C., and Dryer, Murray: Comparison at Supersonic Speeds of Translating Spike Inlets Having Blunt- and Sharp-Lip Cowls. NACA RM E54J07, 1955.

2. Anderson, Arthur R., and Weinstein, Maynard I.: Aerodynamic Performance of Several Techniques for Spike Position Control of a Blunt Lip Nose Inlet Having Internal Contraction at Mach Numbers of 0.63 and 1.5 to 2.0. NACA RM E57D15, 1957.

3. Musial, Norman T., and Bowditch, David: Effects of Free-Stream Reynolds Number, Engine Installation, and Model Scale on Stability Characteristics of a Translating-Spike Inlet at Mach Number 2.0. NACA RM E57D17, 1957.

4. Beheim, Milton A., and Englert, Gerald W.: Effects of a J34 Turbojet Engine on Supersonic Diffuser Performance. NACA RM E55I21, 1956.

5. Piercy, Thomas G., and Chiccine, Bruce G.: Development of Flow Distortions in a Full-Scale Nacelle Inlet at Mach Numbers of 0.63 and 1.6 to 2.0. NACA RM E56G13a, 1956.

6. Fox, Jerome L.: Supersonic Tunnel Investigation by Means of Inclined-Plate Technique to Determine Performance of Several Nose Inlets over Mach Number Range of 1.72 to 2.18. NACA RM E50K14, 1951.

7. Sibulkin, Merwin: Theoretical and Experimental Investigation of Additive Drag. NACA Rep. 1187, 1954. (Supersedes NACA RM E51B13.)

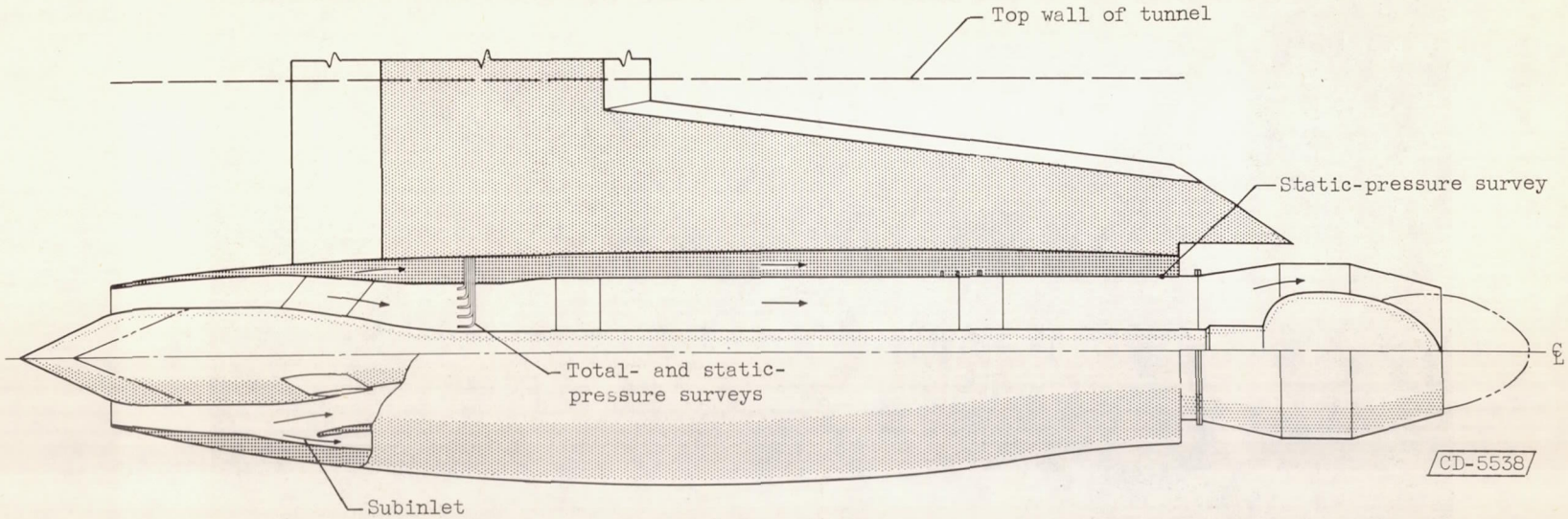

(a) Schematic drawing.

Figure 1. - Nacelle installed in 10- by 10-foot supersonic wind tunnel.

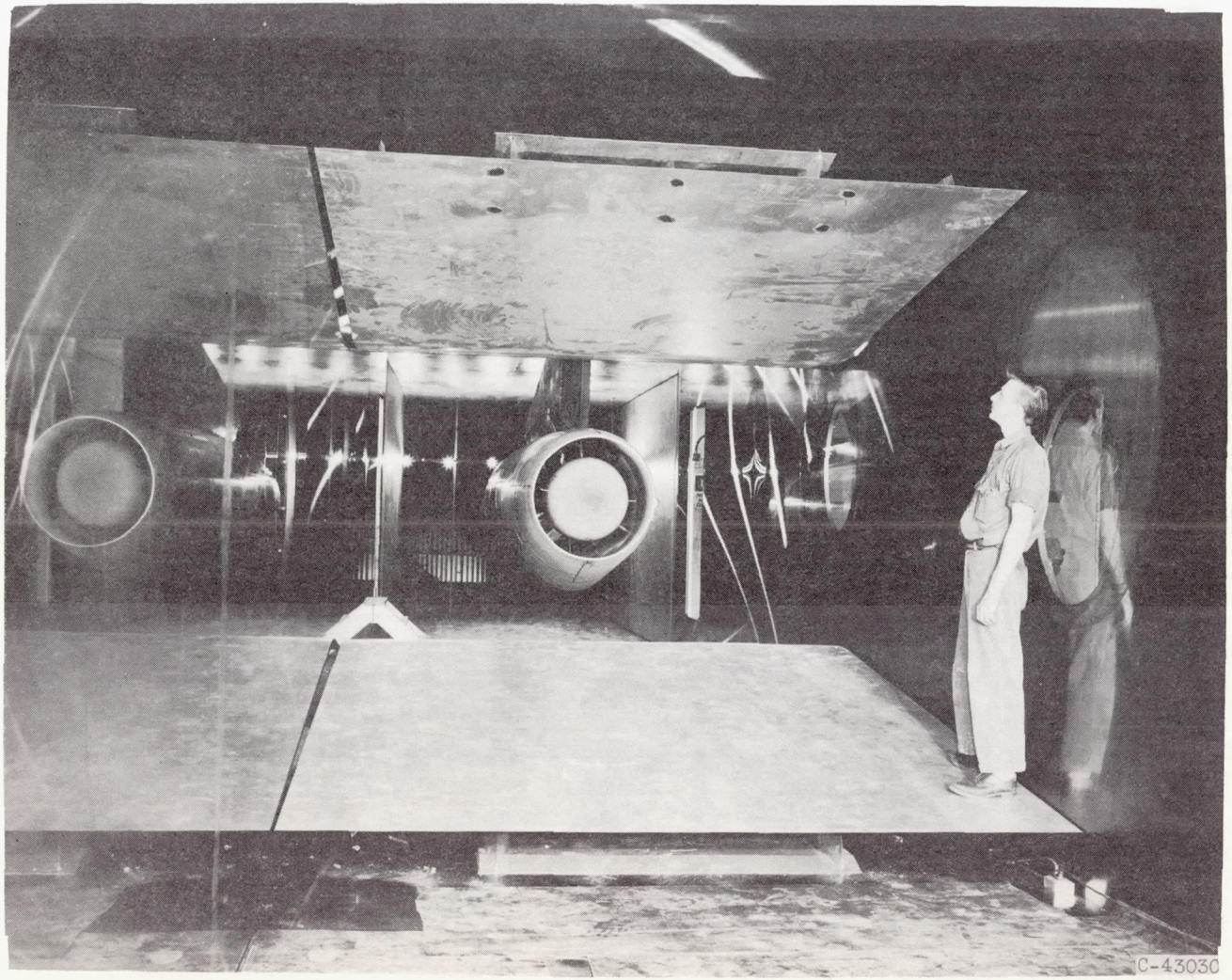

(b) Compression plates.

Figure 1. - Concluded. Nacelle installed in 10- by 10-foot supersonic wind tunnel.

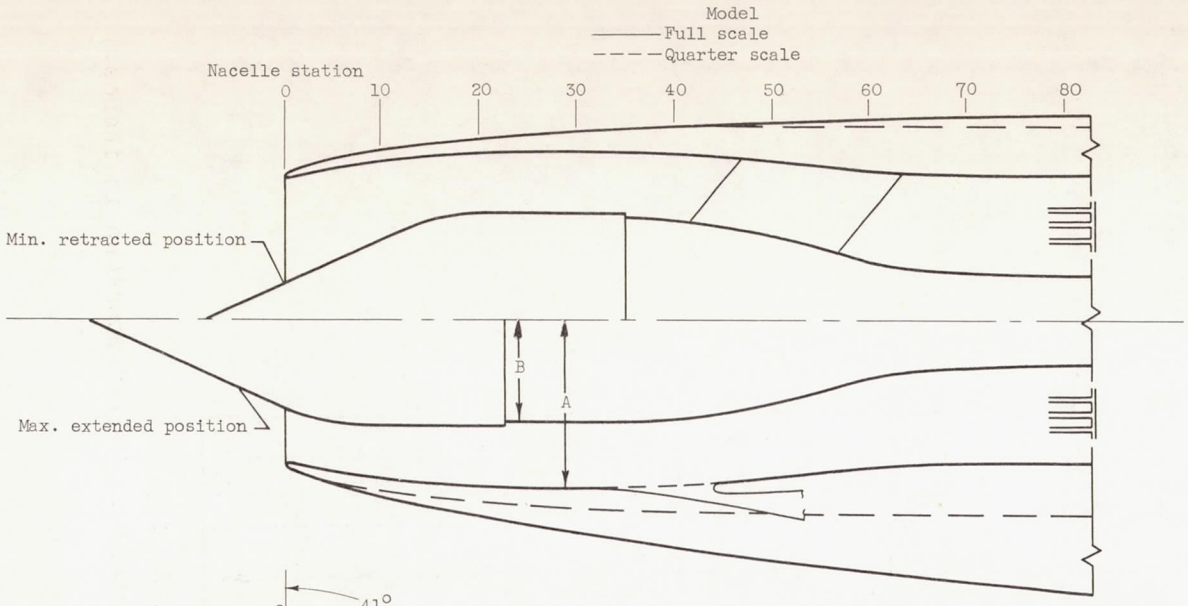

Inlet coordinates

Station	A	B
2.4	15.290	
5.4	15.820	
9.4	16.181	
13.4	16.500	10.900
17.4	16.727	10.900
27.4	17.094	10.720
37.4	17.414	10.700
47.4	16.940	9.500
57.4	16.015	7.350
67.4	15.389	5.500
77.4	15.216	4.800
82.4	15.200	4.750

Cowl coordinates

Station	Upper	Lower
7.4	17.00	17.20
17.4	18.10	19.30
27.4	18.90	21.18
37.4	19.50	22.90
47.4	20.00	24.30
57.4	20.35	25.60
67.4	20.70	26.70
77.4	21.00	27.60

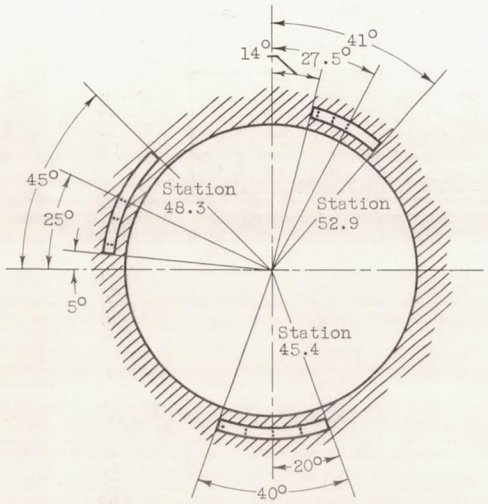

Location of subinlets viewed through throat.

+ Total pressure rake
• Static-pressure taps

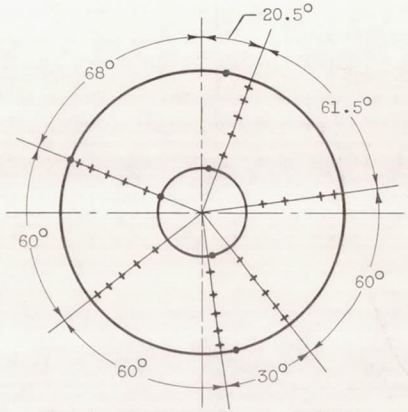

Total-pressure rake at station 78.4; static-pressure taps at station 75.4.

(a) Diffuser and subinlets.

CD-5633

Figure 2. - Inlet details. (All dimensions in inches.)

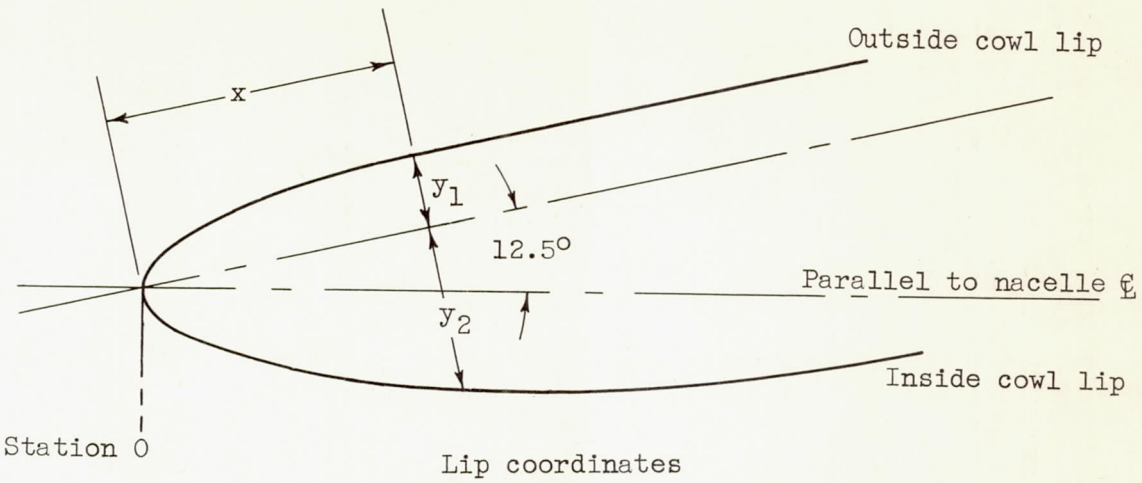

Lip coordinates

x	y_1	y_2
0	0	0
.010	.030	.036
.025	.047	.084
.050	.065	.118
.100	.092	.159
.150	.114	.195
.200	.131	.225
.250	.146	.250
.300	.158	.276
.400	.176	.318
.500	.188	.360
.600	.196	.399
.720	.200	.431
.800	↓	.450
.900		.474
1.000		.492
1.250		.537
1.500		.564
1.750		.585
2.000		.596
2.160		.600

(b) Blunt lip.

Figure 2. - Concluded. Inlet details. (All dimensions in inches.)

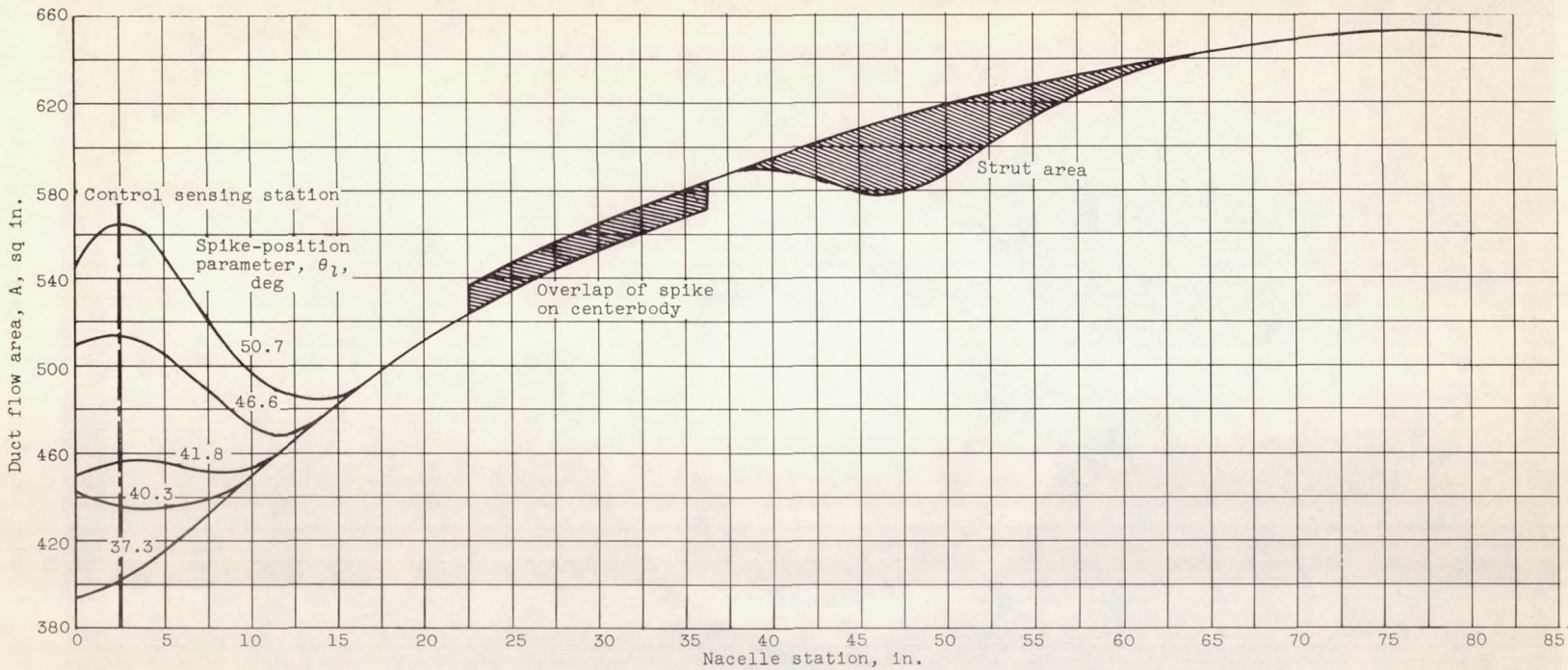

Figure 3. - Internal flow-area distribution. (Station 0 located at vertical tangent to cowl lip.)

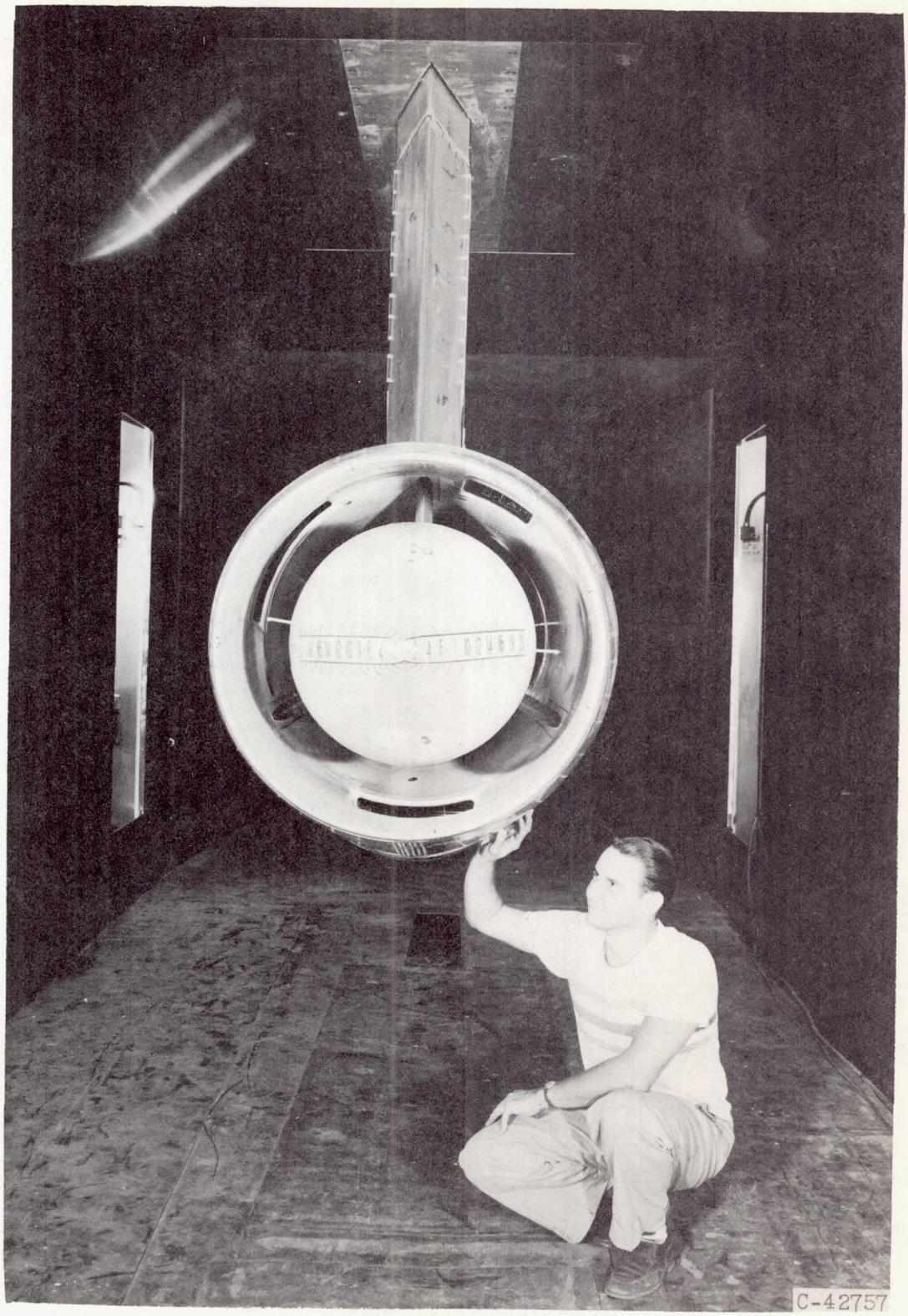

Figure 4. - Main inlet showing circumferential location of subinlets.

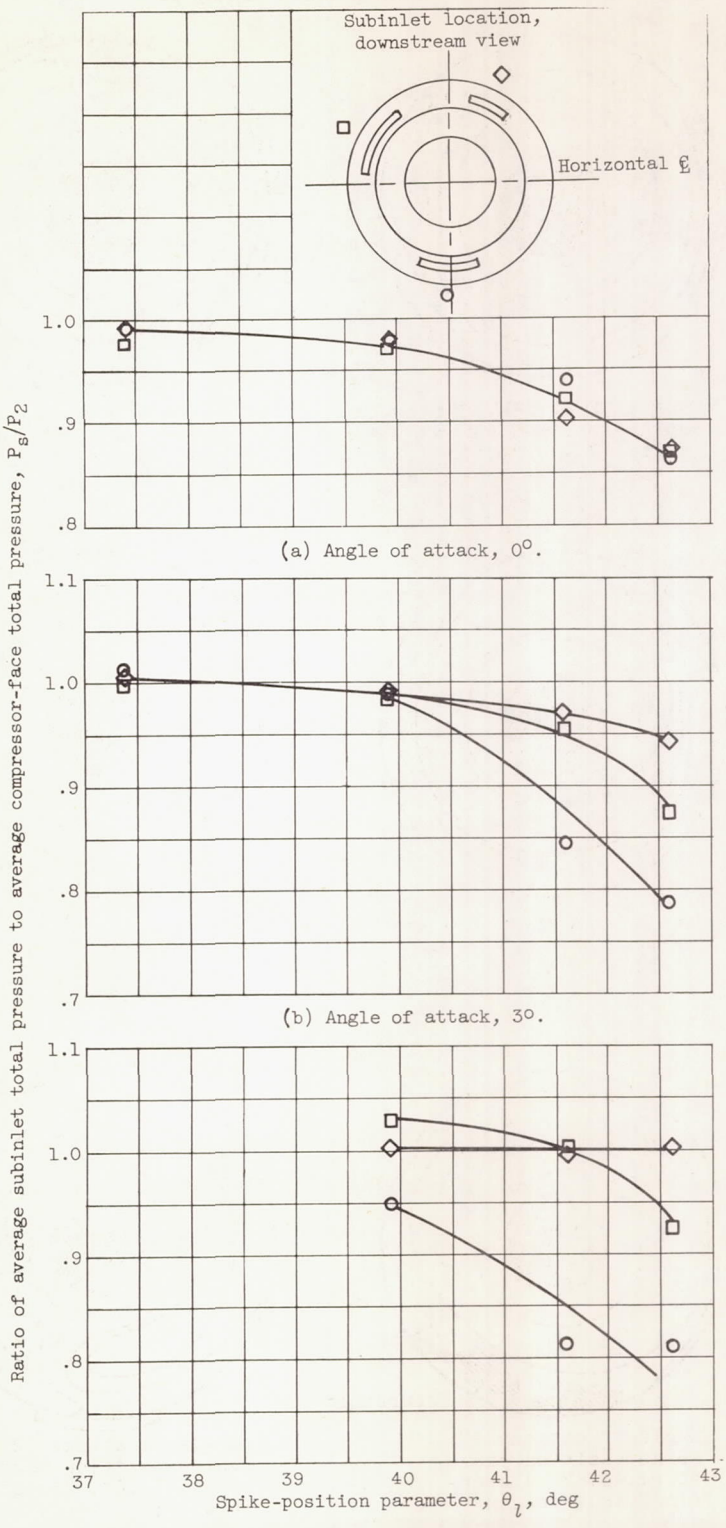

(a) Angle of attack, 0°.

(b) Angle of attack, 3°.

(c) Angle of attack, 6°.

Figure 5. - Performance of subinlets during critical operation of main inlet. Free-stream Mach number, 2.0.

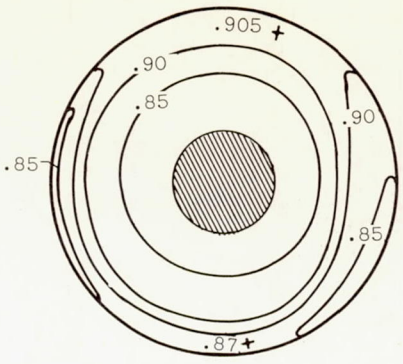

Angle of attack, 0°; spike-position parameter, 37.4°; distortion, 12.0 percent

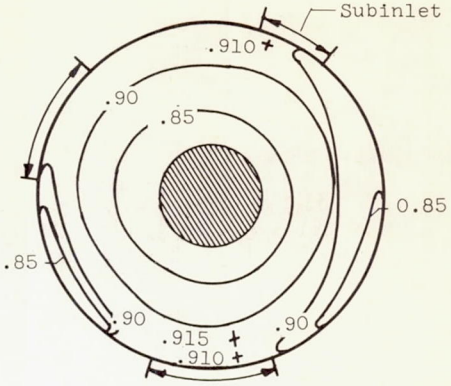

Angle of attack, 0°; spike-position parameter, 37.4°; distortion, 9.4 percent

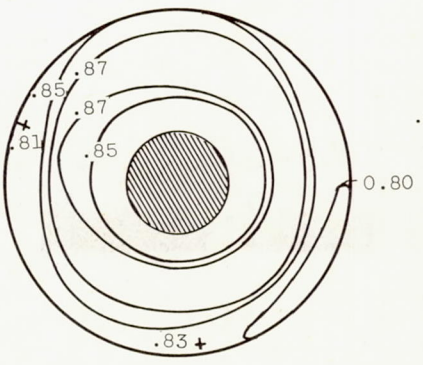

Angle of attack, 0°; spike-position parameter, 41.6°; distortion, 11.1 percent

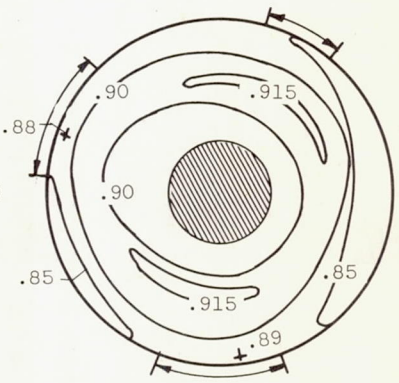

Angle of attack, 0°; spike-position parameter, 41.6°; distortion, 10.9 percent

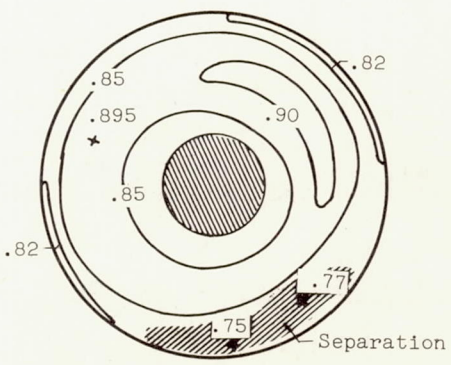

Angle of attack, 6°; spike-position parameter, 41.6°: distortion, 18.2 percent

(a) Subinlets closed.

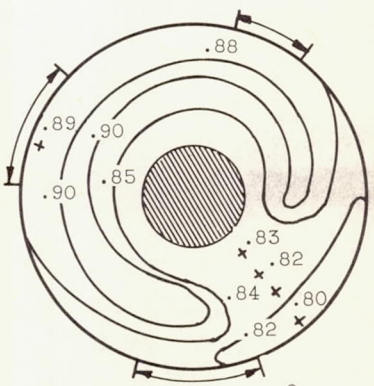

Angle of attack, 6°; spike-position parameter, 41.6°; distortion, 12.0 percent

(b) Subinlets open.

Figure 6. - Effect of subinlets on local total-pressure recovery profiles at compressor face. Inlet operating near critical condition.

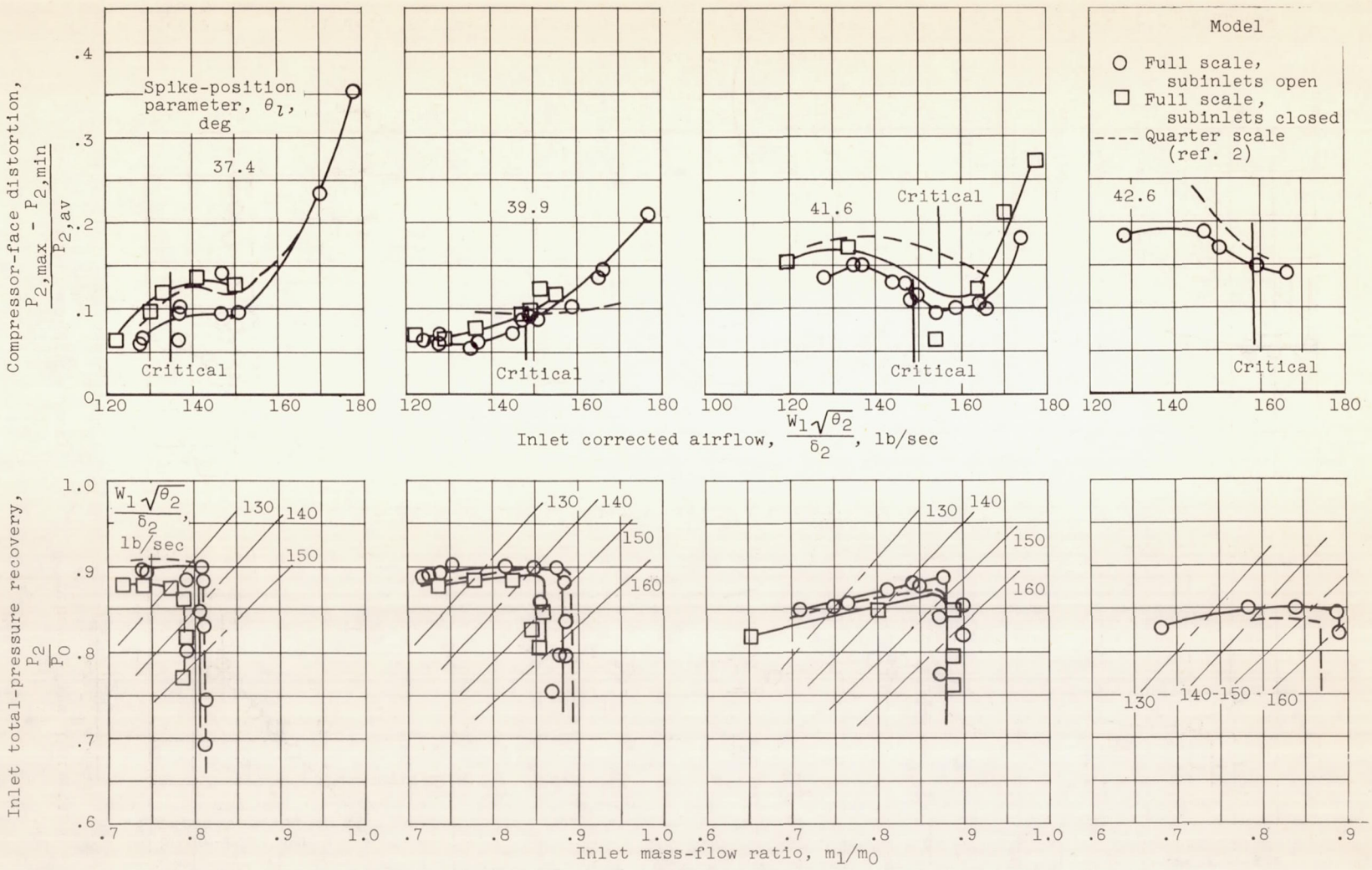

(a) Angle of attack, 0°.

Figure 7. - Full-scale inlet performance compared with quarter-scale results at free-stream Mach number of 2.0.

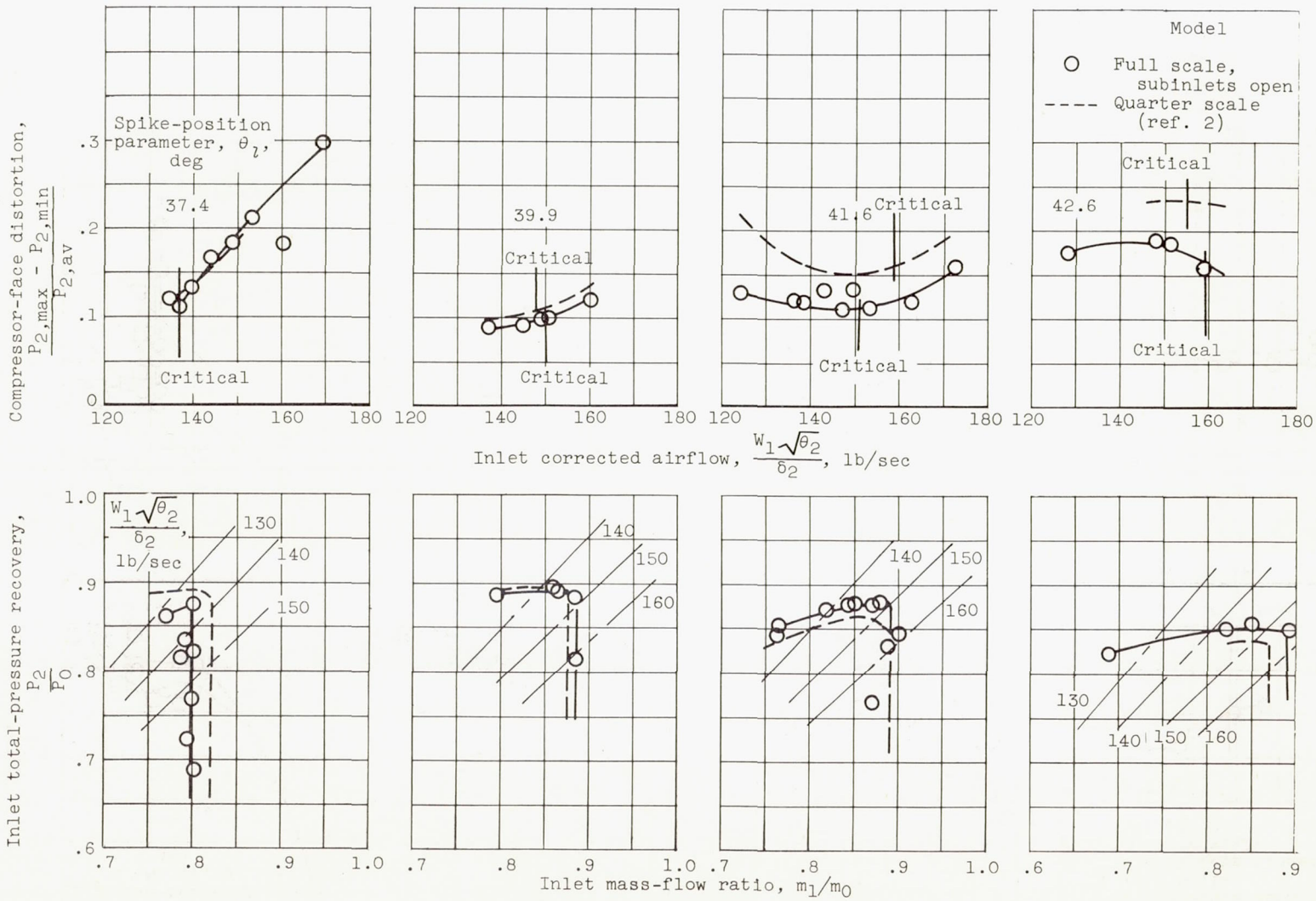

(b) Angle of attack, 3°.

Figure 7. - Continued. Full-scale inlet performance compared with quarter-scale results at free-stream Mach number of 2.0.

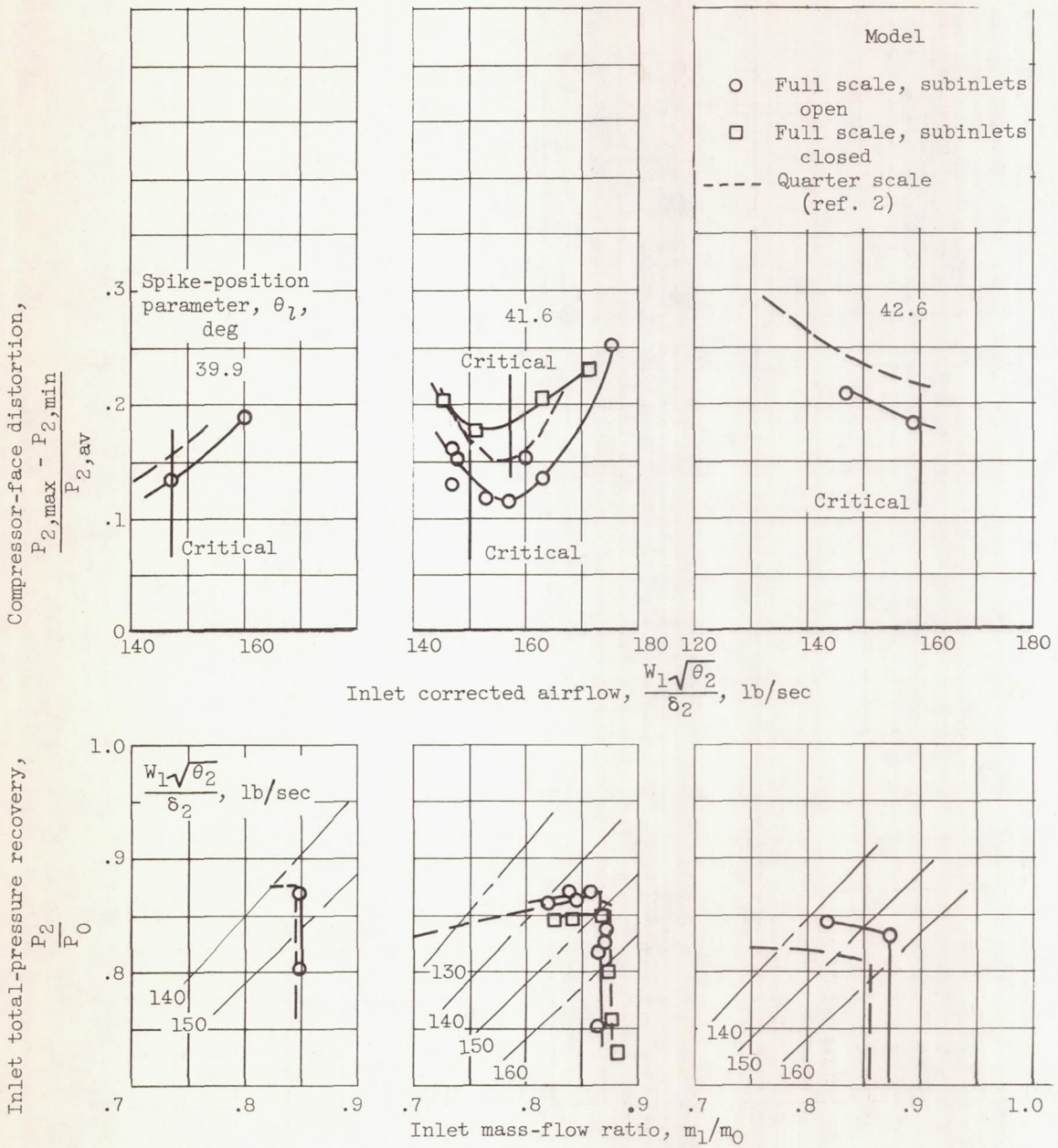

(c) Angle of attack, 6°.

Figure 7. - Concluded. Full-scale inlet performance compared with quarter-scale results at free-stream Mach number of 2.0.

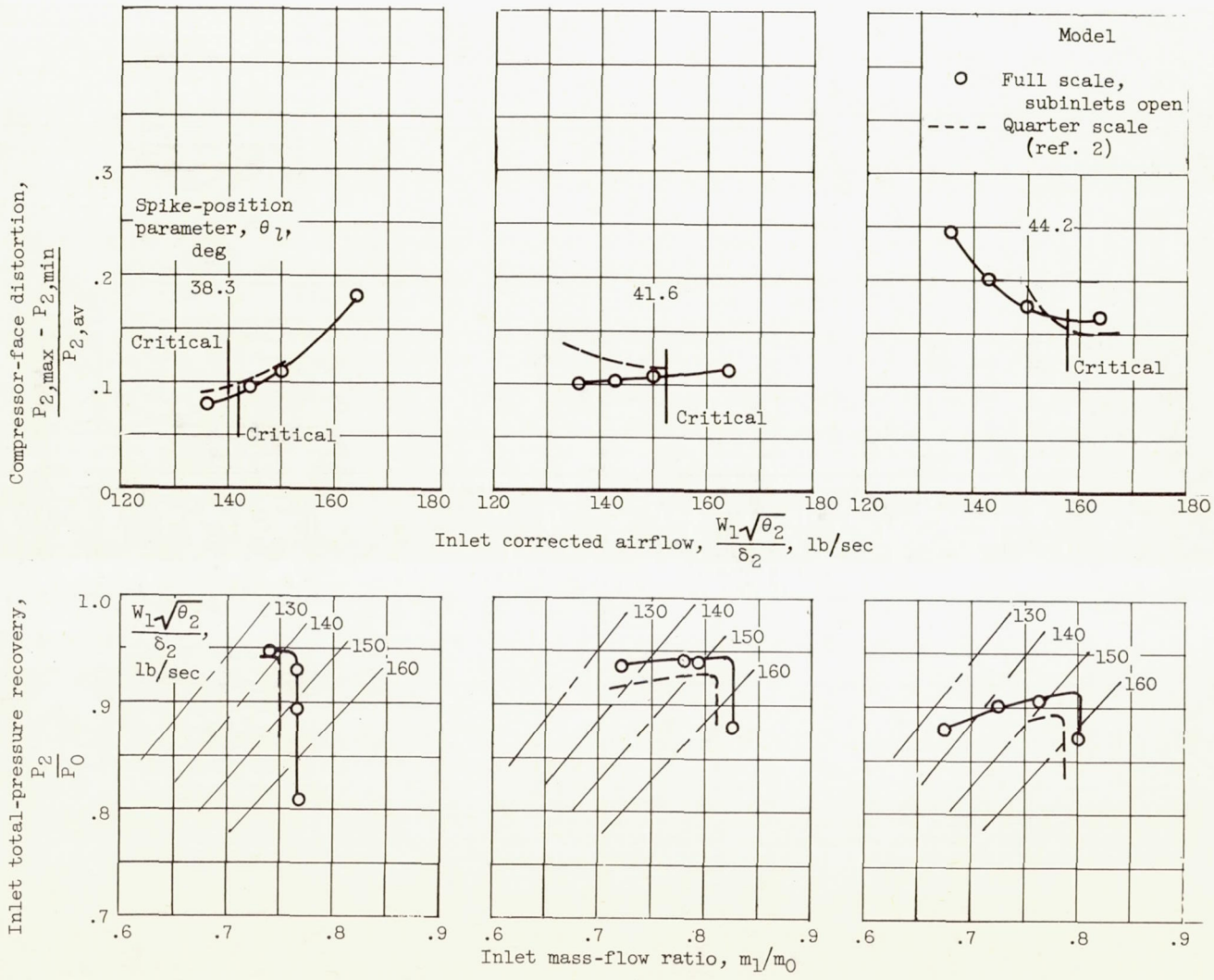

(a) Angle of attack, 0°.

Figure 8. - Full-scale inlet performance compared with quarter-scale results at free-stream Mach number of 1.8.

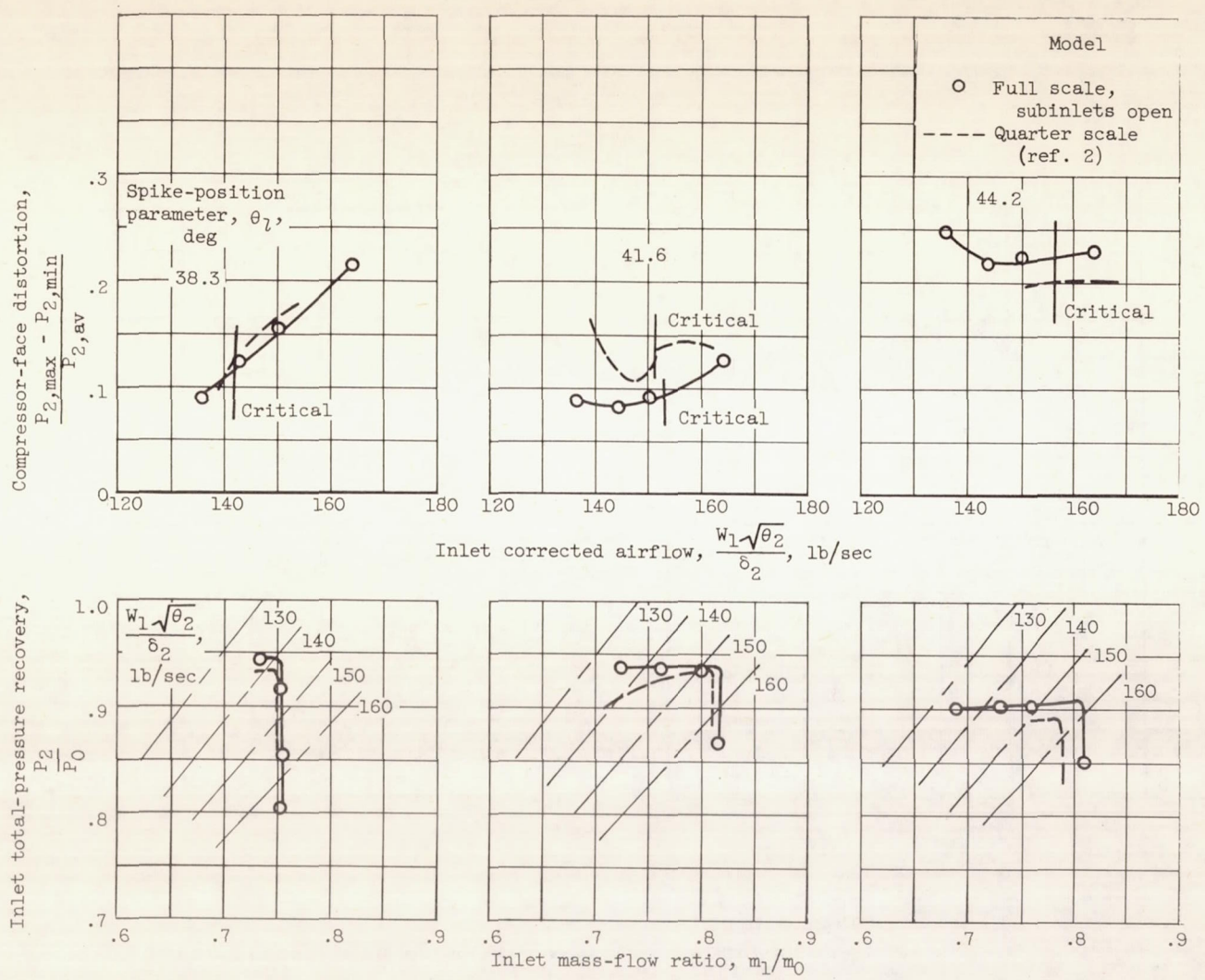

(b) Angle of attack, 3°.

Figure 8. - Continued. Full-scale inlet performance compared with quarter-scale results at free-stream Mach number of 1.8.

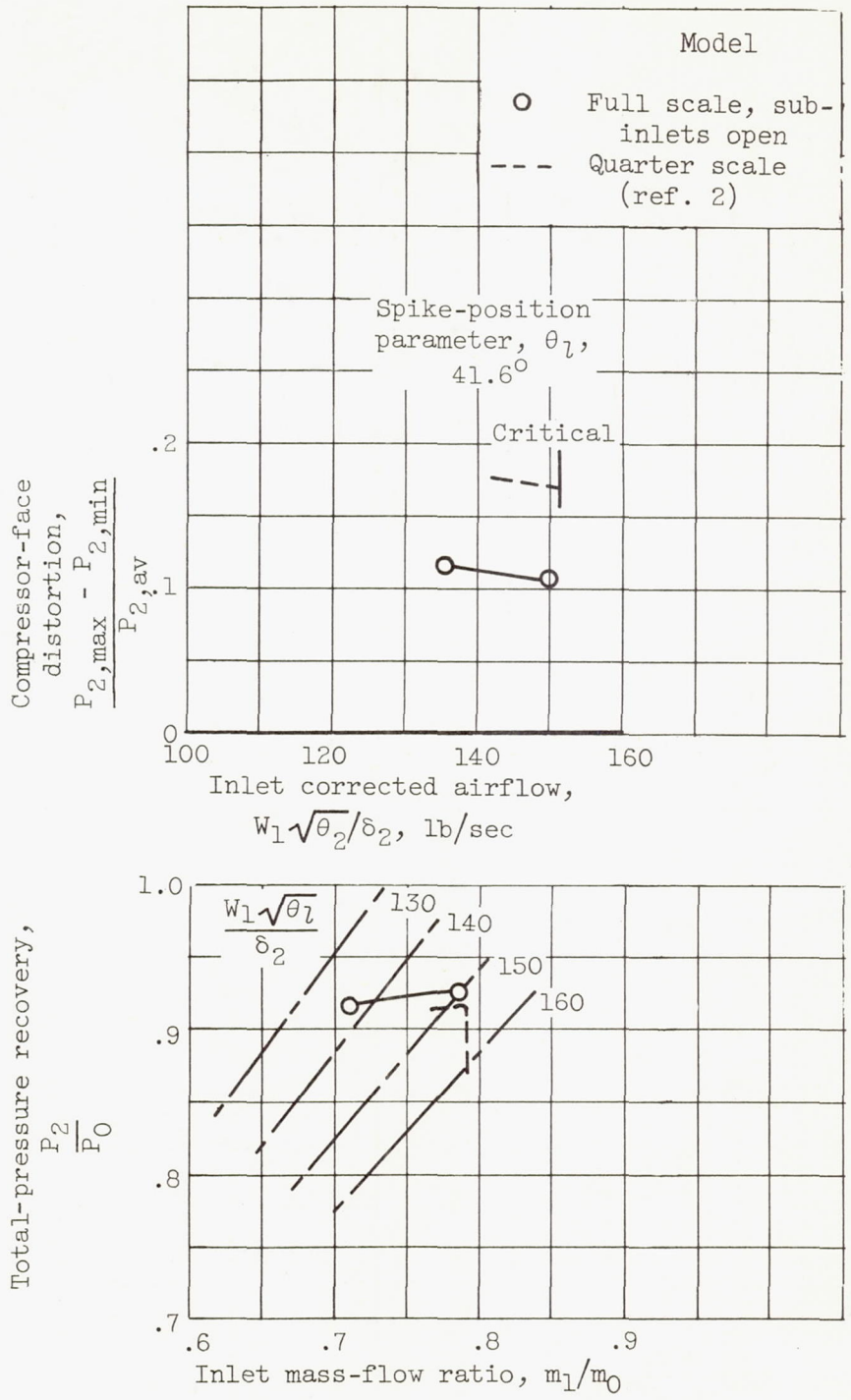

(c) Angle of attack, 6°.

Figure 8. - Concluded. Full-scale inlet performance compared with quarter-scale results at free-stream Mach number of 1.8.

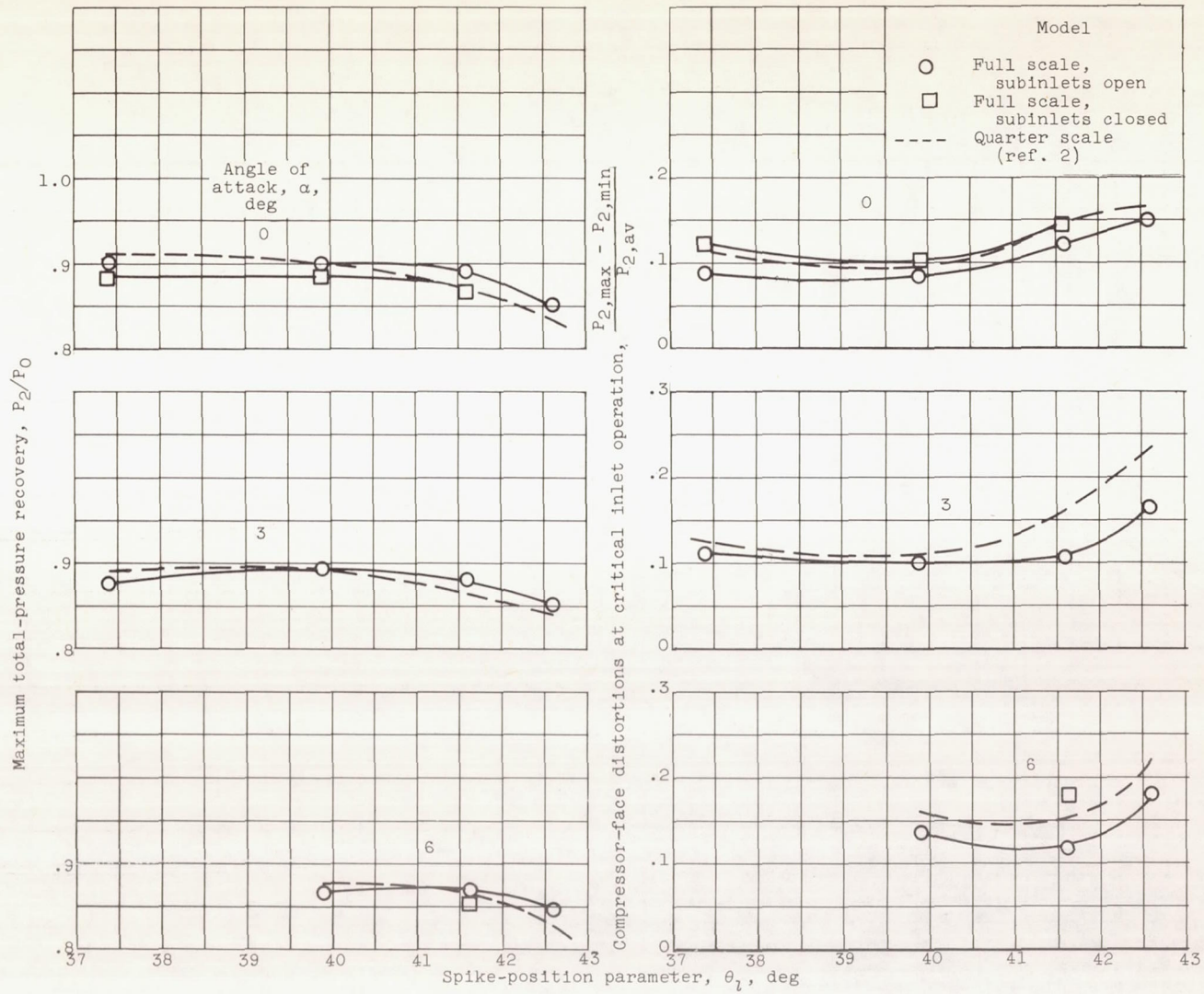

(a) Free-stream Mach number, 2.0.

Figure 9. - Effect of spike position on inlet performance.

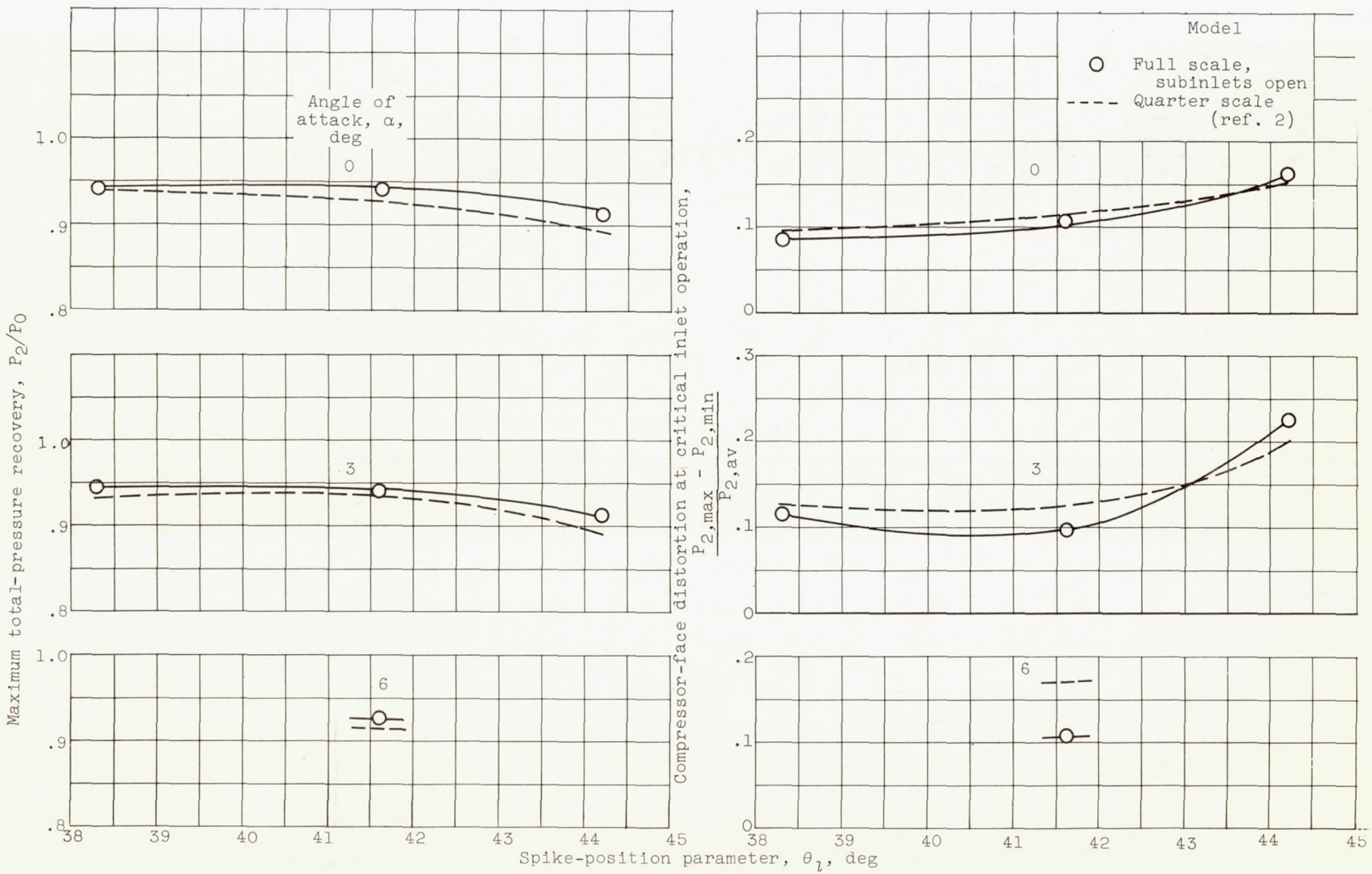

(b) Free-stream Mach number, 1.8.

Figure 9. - Concluded. Effect of spike position on inlet performance.

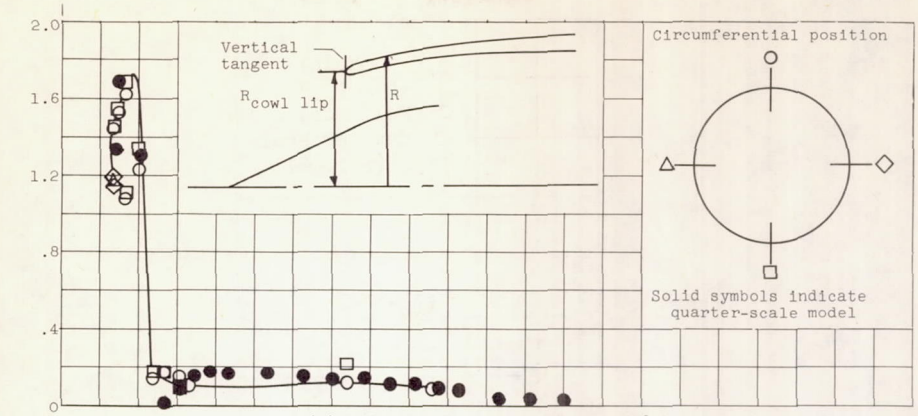

(a) Spike-position parameter, 41.6°.

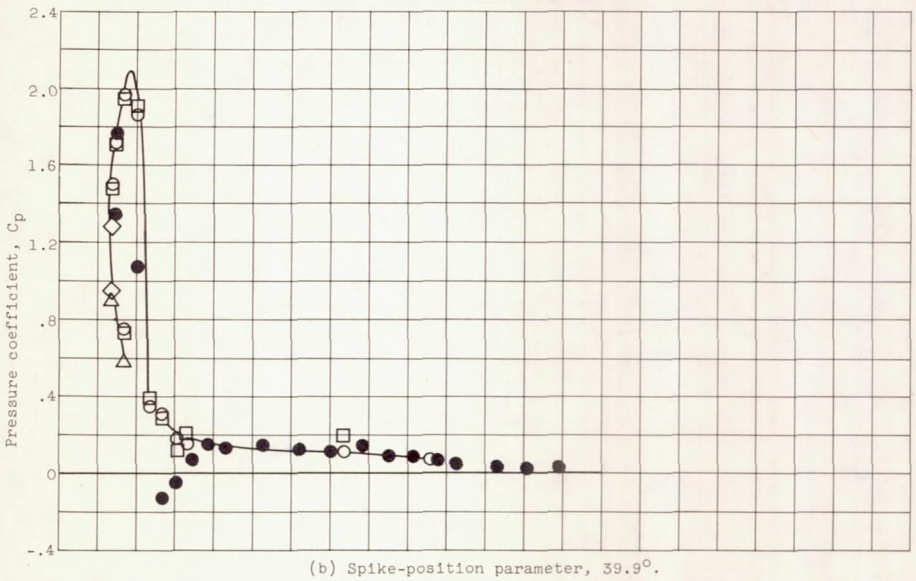

(b) Spike-position parameter, 39.9°.

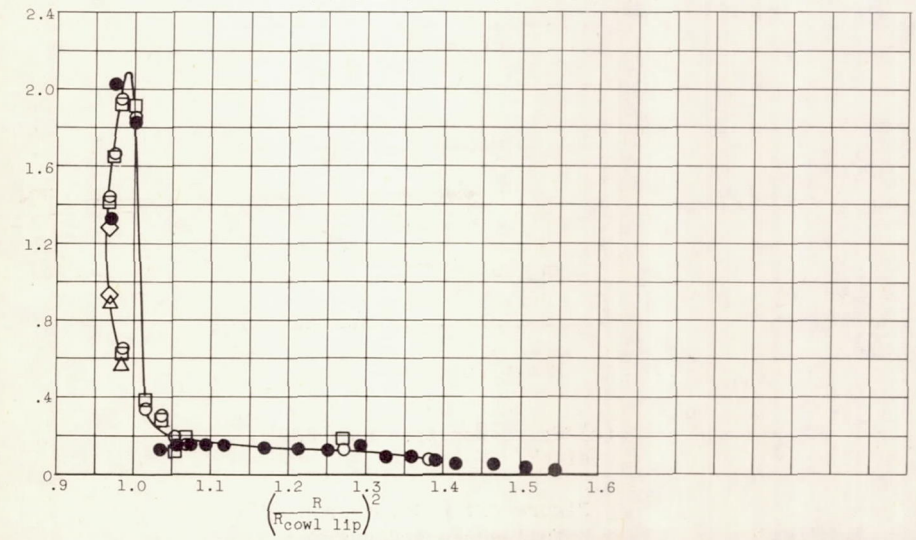

(c) Spike position parameter, 37.4°.

Figure 10. - Comparison of full-scale and quarter-scale pressure distributions on cowl lip at supercritical inlet operation. Free-stream Mach number, 2.0; angle of attack, 0°.

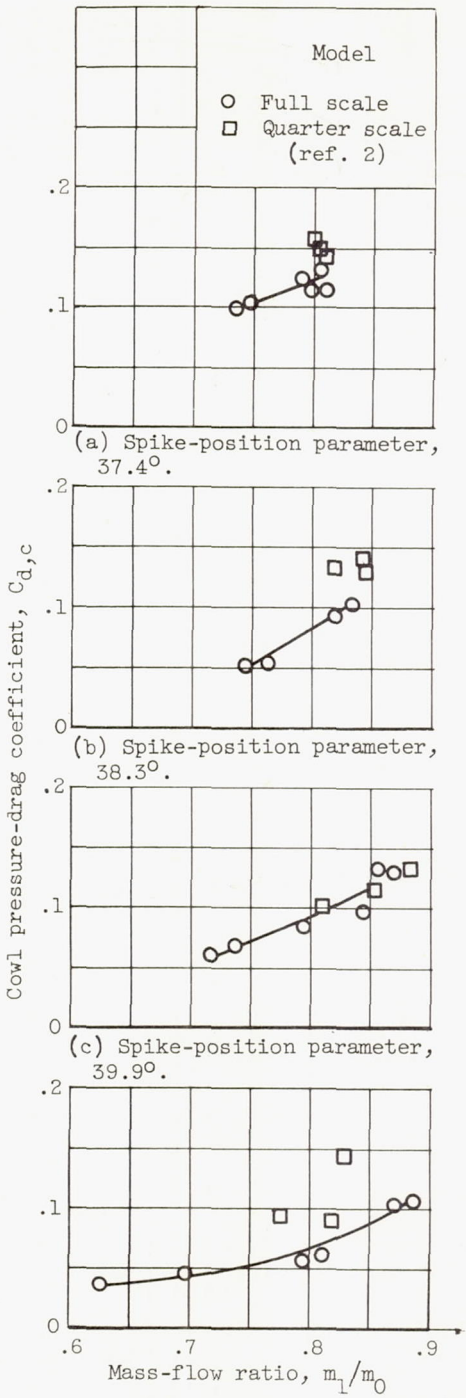

(a) Spike-position parameter, 37.4°.

(b) Spike-position parameter, 38.3°.

(c) Spike-position parameter, 39.9°.

(d) Spike-position parameter, 41.6°.

Figure 11. - Comparison of full-scale and quarter-scale cowl pressure drags. Free-stream Mach number, 2.0; angle of attack, 0°.

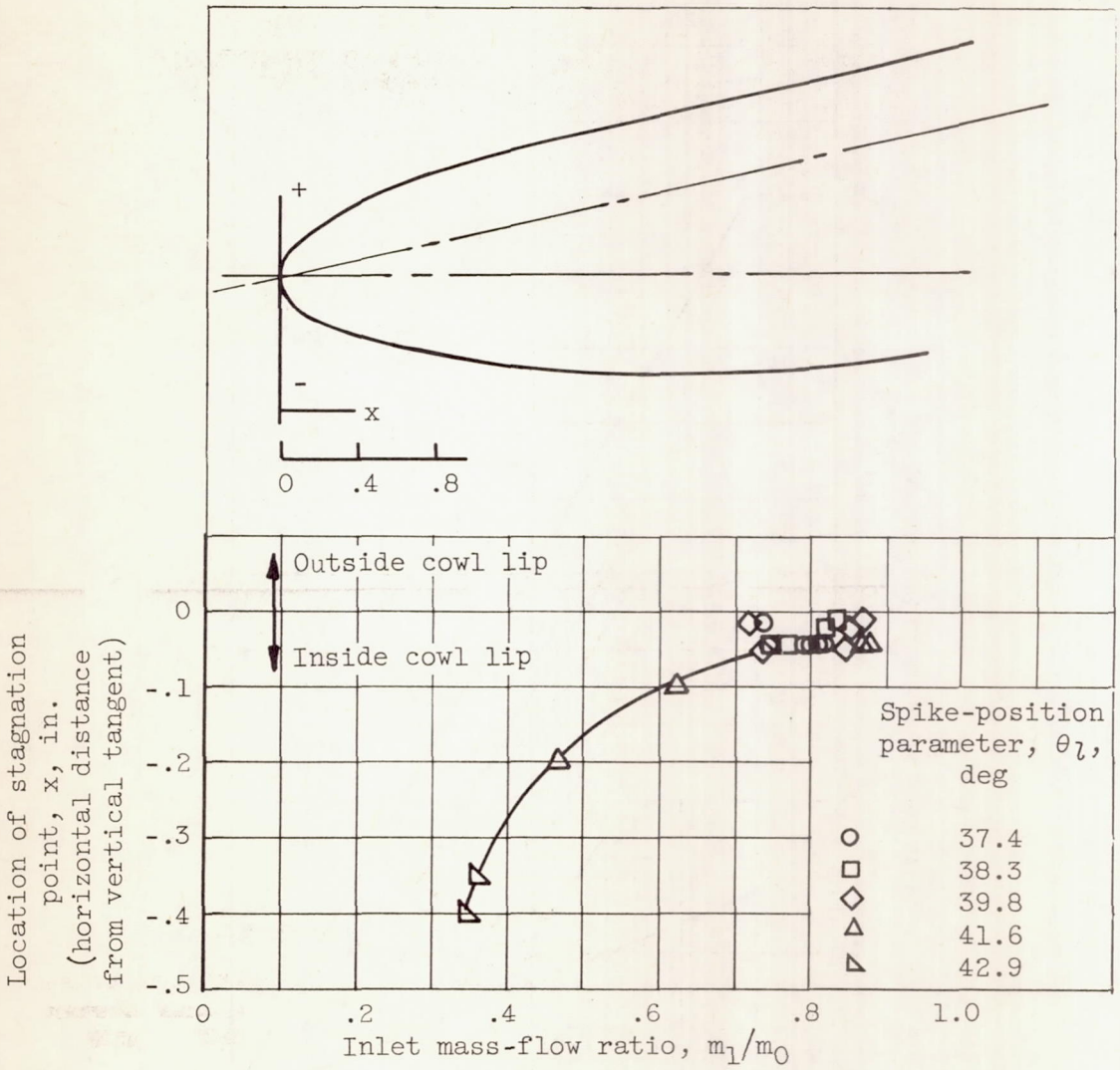

Figure 12. - Effect of mass-flow ratio on location of stagnation point on blunt lip. Free-stream Mach number, 2.0; angle of attack, 0°.

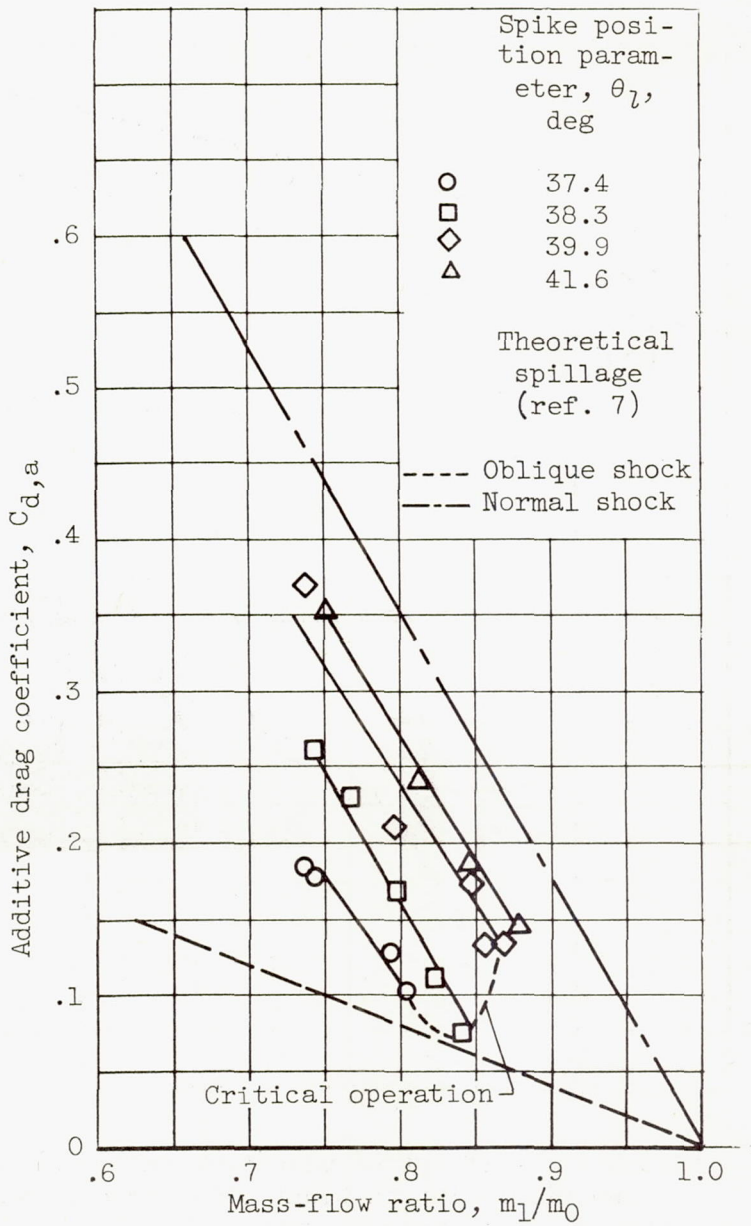

Figure 13. - Additive-drag characteristics. Free-stream Mach number, 2.0; angle of attack, 0°.

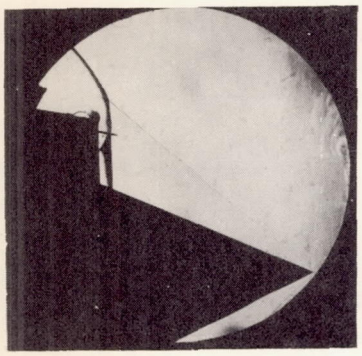

Spike-position parameter, 37.4°; inlet mass-flow ratio, 0.810

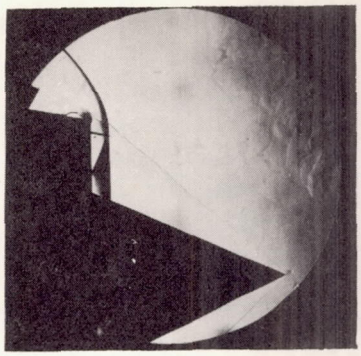

Spike-position parameter, 39.9°; inlet mass-flow ratio, 0.870

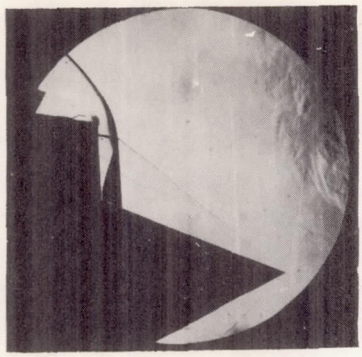

Spike-position parameter, 41.6°; inlet mass-flow ratio, 0.880

(a) Free-stream Mach number, 2.0.

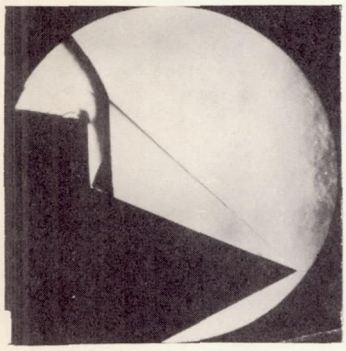

Spike-position parameter, 38.2°; inlet mass-flow ratio, 0.762

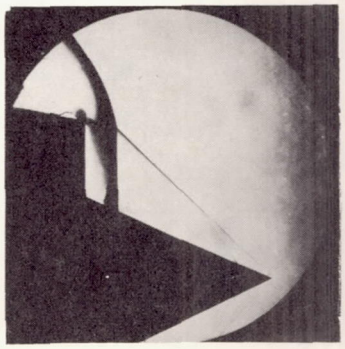

Spike-position parameter, 40.7°; inlet mass-flow ratio, 0.800

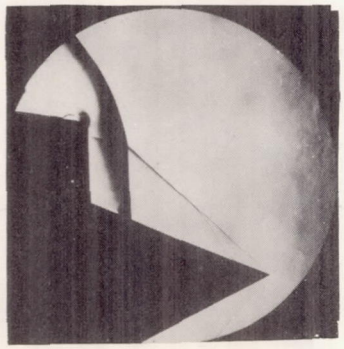

Spike-position parameter, 42.2°; inlet mass-flow ratio, 0.800

(b) Free-stream Mach number, 1.8. C-44755

Figure 14. - Schlieren photos for critical operation. Angle of attack, 0°.